Suspended carbon nanotube nanocomposite beams with a high mechanical strength via layer-by-layer nano-self-assembly

To cite this article: Dongjin Lee and Tianhong Cui 2011 *Nanotechnology* **22** 165601

View the article online for updates and enhancements.

Related content

- Characterization of layer-by-layer self-assembled carbon nanotube multilayer thinfilms
Wei Xue and Tianhong Cui
- Growth and characterization of horizontally suspended CNTs across TiN electrodegaps
Claudia A Santini, Daire J Cott, Ainhoa Romo-Negreira et al.
- Polymer nanocomposite nanomechanical cantilever sensors: material characterization,device development and application in explosive vapour detection
V Seena, Avil Fernandes, Prita Pant et al.

Recent citations

- Carbon nanotube network varactor
A A Generalov *et al*

IOP ebooks™

Bringing you innovative digital publishing with leading voices to create your essential collection of books in STEM research.

Start exploring the collection - download the first chapter of every title for free.

This content was downloaded from IP address 131.212.250.26 on 25/09/2019 at 01:00

Nanotechnology **22** (2011) 165601 (9pp) doi:10.1088/0957-4484/22/16/165601

Suspended carbon nanotube nanocomposite beams with a high mechanical strength via layer-by-layer nano-self-assembly

Dongjin Lee and Tianhong Cui[1]

Department of Mechanical Engineering, University of Minnesota, 111 Church Street SE, Minneapolis, MN 55455, USA

E-mail: tcui@me.umn.edu

Received 27 November 2010, in final form 4 February 2011
Published 11 March 2011
Online at stacks.iop.org/Nano/22/165601

Abstract

The fabrication and characterization of single-walled carbon nanotube (SWCNT) composite thin film micropatterns and suspended beams prepared by lithography-compatible layer-by-layer (LbL) nano-self-assembly are demonstrated. Negatively charged SWCNTs are assembled with a positively charged polydiallyldimethylammonium chloride, and the composite thin film is patterned by oxygen plasma etching with a masking layer of photoresist, resulting in a feature size of 2 μm. Furthermore, the SWCNT nanocomposite stripe pattern with a metal clamp on both ends is released by etching a sacrificial layer of silicon dioxide in the hydrofluoric acid vapor. I–V measurement reveals that the resistance of SWCNT nanocomposite film decreases by 23% upon release, presumably due to the effect of reorientation of CNTs caused by the deflection of about 50 nm. A high Young's modulus is found in a range of 500–800 GPa based on the characterization of a fixed–fixed beam using nanoindentation. This value is much higher than those of the other CNT–polymer composites reported due to organization of structures by self-assembly and higher loading of CNTs. The stiff CNT–polymer composite thin film micropattern and suspended beam have potential applications to novel physical sensors, nanoelectromechanical switches, other M/NEMS devices, etc.

(Some figures in this article are in colour only in the electronic version)

1. Introduction

Carbon nanotubes (CNTs) have been of great interest as a functional nanomaterial for the past two decades due to their extraordinary mechanical, electrical, and optical properties with excellent thermal and chemical stability [1]. It has been suggested that CNTs could be utilized as potential active components such as electrically conducting nanoscale wires [2], semiconducting channel materials for transistors [3, 4], and sensing elements [5, 6], etc. In order to fully exploit these properties, however, CNTs need to be assembled into existing devices or matrix materials in conjunction with a high degree of controllability and compatibility with extant fabrication technologies [7]. The integration of CNTs as a functional element in microfabricated devices is of great interest in the field of nanoelectronics and nanoelectromechanical systems (NEMS). Although synthetic incorporation methods, such as *in situ* growth of individual CNTs [8] over two anchoring pads and a CNT forest [9] aligned perpendicularly to the substrate, possess a high degree of controllability in alignment, they are counteracted by the harsh environment and long process time, which reduce compatibility with existing device technologies. Furthermore, careful manipulation of catalytic metal nanoparticles is required for a patterned or ordered architecture [7]. On the other hand, post-synthetic approaches are advantageous with

[1] Address for correspondence: Department of Mechanical Engineering, University of Minnesota at Twin Cities, USA.

 © 2011 IOP Publishing Ltd Printed in the UK & the USA

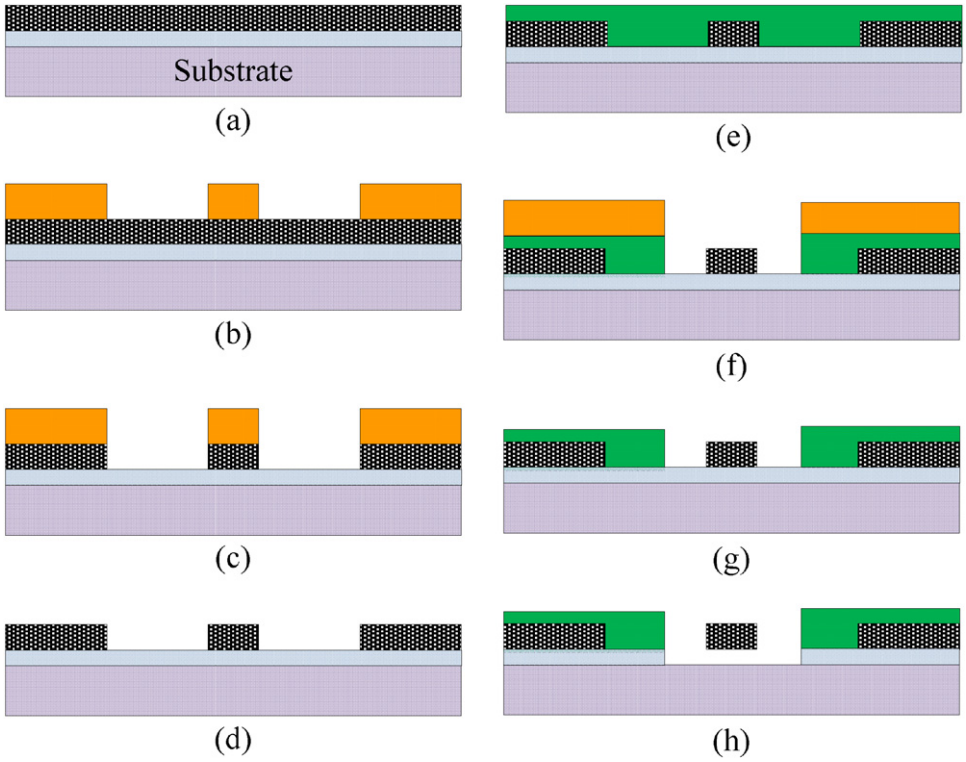

Figure 1. Process flow chart for the fabrication of micropatterns (left) and suspended beams (right): (a) LbL assembly of CNT on Si/SiO_2 substrate, (b) photoresist (PR) patterning as a mask for CNT thin film etching, (c) CNT film etching with O_2 plasma, (d) PR strip, (e) sputter deposition of (Cr/Au) as a metal pad, (f) metal etching, (g) PR strip, and (h) sacrificial layer of SiO_2 etching in a HF vapor tank: the fabrication of micropatterns and suspended beams is achieved by lithographically-compatible processes.

regard to cost and time aspects. They also enable large-scale production which promotes future commercialization of CNT-based devices. Moreover, post-growth approaches accomplish facile assembly accompanied by the horizontal alignment and patterning of thin film [10, 11], which can be integrated into existing technologies.

The combination of the intrinsic properties of CNTs with a low density triggered research on CNT–polymer composites for structural reinforcement, enhancement of electrical [12] and thermal conductivity [13, 14], and adjustment of optical properties [15]. Theoretical work [16, 17] has revealed that CNTs are among the stiffest and strongest materials ever known, with a modulus of more than 1 TPa and a tensile strength of up to 150 GPa. Consequently, much research has been done to explore CNTs as a next-generation composite material. In order to manufacture CNT–polymer composites, solvent casting [18, 19], melt blending [20], and *in situ* polymerization [21] have been widely used, depending on the method of incorporation of CNTs into the host polymer matrix. Along with the Langmuir–Blodgett method [22], layer-by-layer (LbL) assembly has been used to manufacture ultra-thin film as a functional material [23–25] with controlled internal structures. In addition, LbL assembly is an environmentally sound and potentially cost-effective method. Furthermore, it can be performed on substrates of various sizes, shapes, and materials. Since the first pioneering research on LbL self-assembly of CNTs [23], this method has emerged as an alternative method for integrating CNTs into devices or versatile functional materials without any segregation. A multilayer of SWCNT–polyethyleneimine was reported to have an elastic modulus of 35 GPa and tensile strength of up to 325 MPa [23] in a tensile test. LbL assembly of CNTs becomes more advantageous, because CNTs are considered as low-cost off-the-shelf building blocks thanks to today's large-scale production of CNTs. Research on the lithographic micropatterning of LbL assembled nanomaterial multilayer has been reported for nanoparticle [10] and CNT multilayers, where a 5 μm feature size was obtained using lift-off technique [11]. Also, CNT film patterning was reported using photoablation with an excimer laser [26]. In this work we used molecular LbL assembly to fabricate functional thin film micropatterns and suspended beams. To the best of our knowledge, nanomaterial-based suspended films have not been reported yet.

The fabrication and characterization of SWCNT nanocomposite film micropatterns and suspended beams are demonstrated by facile, low-cost, and lithographically-compatible LbL assembly. The SWCNT nanocomposite film was etched out using oxygen plasma dry etching and characterized with scanning electron microscopy (SEM) and Raman spectroscopy to ensure that SWCNTs were completely removed in the etched region. Indeed, a feature size of 2 μm was obtained by oxygen (O_2) plasma etching with a photoresist mask. A sacrificial layer of silicon dioxide grown by plasma enhanced chemical vapor deposition (PECVD) was etched in hydrofluoric acid (HF) vapor to avoid stiction, and the patterned SWCNT composite

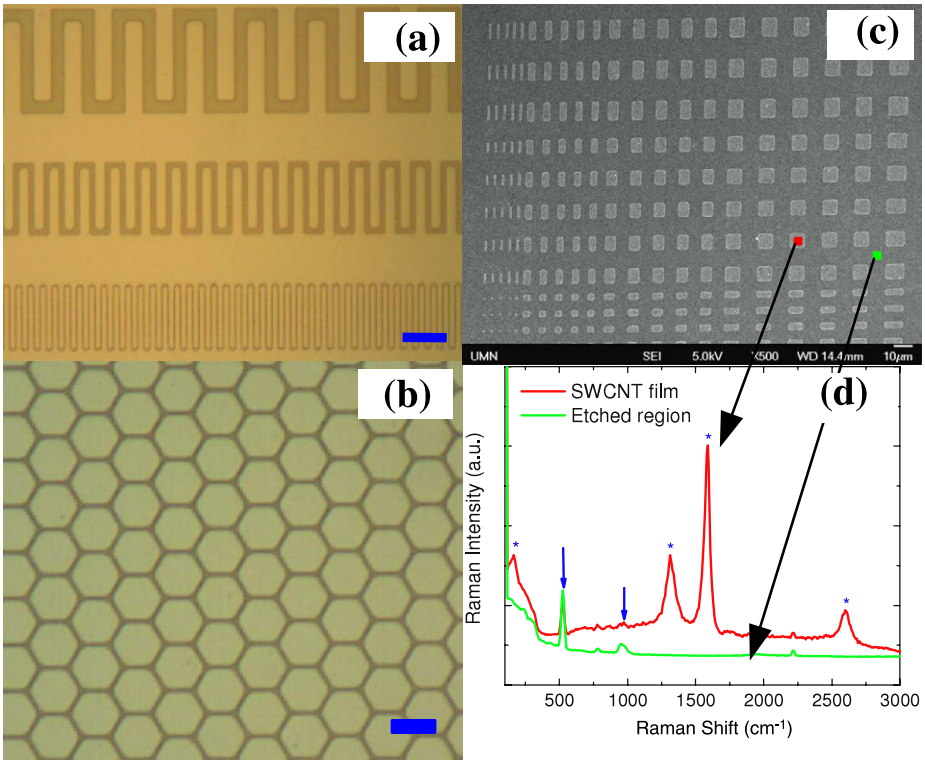

Figure 2. LbL assembled SWCNT thin film micropatterns by means of O_2 plasma dry etching (scale bars: 30 μm) with a photoresist mask: optical images of 2, 5, and 10 wide stripes (a) and honeycomb pattern with 4 μm wide stripe (b), (c) SEM image of square dot grid pattern, and (d) Raman spectra on the SWCNT thin film patterns and etched region. The feature size of 2 μm is clearly observed. Raman spectra show no G-, D-, or G′-bands on the etched region, meaning that SWCNTs have been completely removed by the O_2 plasma.

film was successfully released, followed by characterization with SEM and confocal microscopy. The suspended beams were characterized electrically using I–V measurement, and it turned out that the electrical resistance decreased upon release, presumably due to the reorientation of CNTs as a result of a small deflection of 50 nm. The mechanical test yielded a higher Young's modulus of 500–800 GPa than those of the reported CNT–polymer composites under the assumption of an Euler beam with fixed ends. CNT–polymer multilayer composites prepared by molecular LbL assembly are practical and economically viable as one of the stiffest materials available. Furthermore, the suspended CNT–polymer composite film may play a very important role in novel physical sensors, nano-switches, other M/NEMS devices, etc.

2. Experimental section

2.1. Materials and method

Commercially available pristine SWCNTs (1–2 nm in diameter and 50 μm long) were chemically functionalized as done previously [27, 28] in concentrated acid (3:1 H_2SO_4:HNO_3) at 110 °C for 1 h. This resulted in negatively charged hydroxyl (−OH) or carboxylic groups (−COOH) evidenced by Fourier transform infrared spectroscopy demonstrating a strong peak at 1760 cm^{-1} [28]. These hydrophilic groups greatly enhanced the solubility and stability of the aqueous solution of SWCNTs with a concentration of 0.06 wt%. The polyelectrolytes used for LbL assembly as polycation and polyanion were poly(diallyldimethylammonium chloride, PDDA, M_w = 200–350k, Sigma-Aldrich) and poly(styrenesulfonate, PSS, M_w = 70k, Sigma-Aldrich), respectively. The concentration of aqueous PDDA and PSS was 1.4 wt% and 0.3 wt%, respectively, with 0.5 M sodium chloride (NaCl). The dipping time for polyelectrolytes and SWCNTs in LbL assembly is 10 and 15 min, respectively.

2.2. Fabrication of micropatterns and suspended beams

The fabrication procedure for the micropatterns and suspended beams is schematized in figure 1. The left panel is for the micropatterning, while right panel is for the suspended beams after subsequent processes such as metal deposition and sacrificial layer etching. Starting with a silicon (Si) wafer cleaned in piranha solution (3:1 H_2SO_4:H_2O_2) at 120 °C for 20 min, 1.7 μm thick silicon dioxide (SiO_2) was grown using PECVD (Plasma-Therm 340). After the assembly of two bilayers of (PDDA/PSS) as precursor layers on Si/SiO_2 substrate, 10 bilayers of (PDDA/SWCNT) were successively deposited (figure 1(a)). Photoresist was spun onto SWCNT composite film and patterned by photolithography (figure 1(b)). After development, an O_2 plasma (STS etcher) was applied to etch out SWCNT composite film at a power of 150 W and an O_2 flow rate of 100 sccm for 2.5 min (figure 1(c)). Then, the SWCNT composite film micropatterns were obtained after the photoresist strip

(figure 1(d)). Thickness measurement was done using a surface profiler (P-16, KLA Tencor) with a force of about 0.02 N at this step, yielding a thickness of 78 ± 1 nm. Chromium (Cr, 250 Å) and gold (Au, 1000 Å) were sputter-deposited (AJA sputter) for the role of 'electrodes' and 'clamps' for electrical and mechanical characterization, respectively (figure 1(e)). After the patterning of the pad, the metal layer was etched (figure 1(f)), and the sacrificial layer of PECVD grown SiO_2 was etched away in the HF vapor for 90 s (figures 1(g) and (h)), followed by thorough rinsing with isopropanol alcohol (IPA). The suspended beam was dried for 1 min on a hotplate at 80 °C upside down to counteract gravity.

2.3. Characterization

The micropattern of the LbL assembled SWCNT composite film was characterized using an optical microscope and SEM (JEOL 6700) to observe the feature size. In particular, Raman spectroscopy (Alpha 300R, WITec) was used to demonstrate that SWCNTs were completely removed from the exposed area in figure 1(c). The spectra were obtained with a 100× objective at the wavelength of 752.5 nm and a power of 300 mW for 10 s on the SWCNT composite film pattern and etched region. The suspended SWCNT composite film beam was initially inspected by an optical microscope by moving the focal plane back and forth to investigate whether the beam is suspended or not. SEM was also used to confirm that the SWCNT composite film was completely released by observing it at a tilted angle. Confocal microscopy (HS-200, Hyphenated Systems) was used to study the topology of the suspended beam. *I–V* measurement was performed using a semiconductor parameter analyzer (HP4156A) before and after release. A mechanical test with *in situ* two-wire resistance measurement was conducted based on the assumption of a fixed–fixed beam at both ends with a point load using a nanoindenter (TI 900 Triboindenter, Hysitron). The suspended beam was located by scanning the surface, and the indenter tip was placed on the center of the suspended beams, followed by the indentation test, which yielded force–deflection curves. The micropatterned metal electrode was connected to a data logging system (Agilent 34970A Data acquisition/switch unit) using the conducting epoxy for electromechanical characterization during the indentation test.

3. Results and discussion

The SWCNT LbL assembled composite film micropattern fabricated by O_2 plasma dry etching with a photoresist mask is illustrated in figure 2. Optical images of 2, 5, and 10 μm wide stripes and the honeycomb shape of the 4 μm wide stripe are shown in figures 2(a) and (b), respectively. The scale bars in the figures indicate 30 μm. Apparently, a feature size of 2 μm is found, which is smaller than that reported for the lift-off technique [11]. Since LbL assembly usually realizes a conformal coating, it may leave the fence that was adsorbed on the sidewall of the patterned photoresist, which might hamper the formation of a smaller feature size. The SEM image of a square dot grid pattern is shown in figure 2(c).

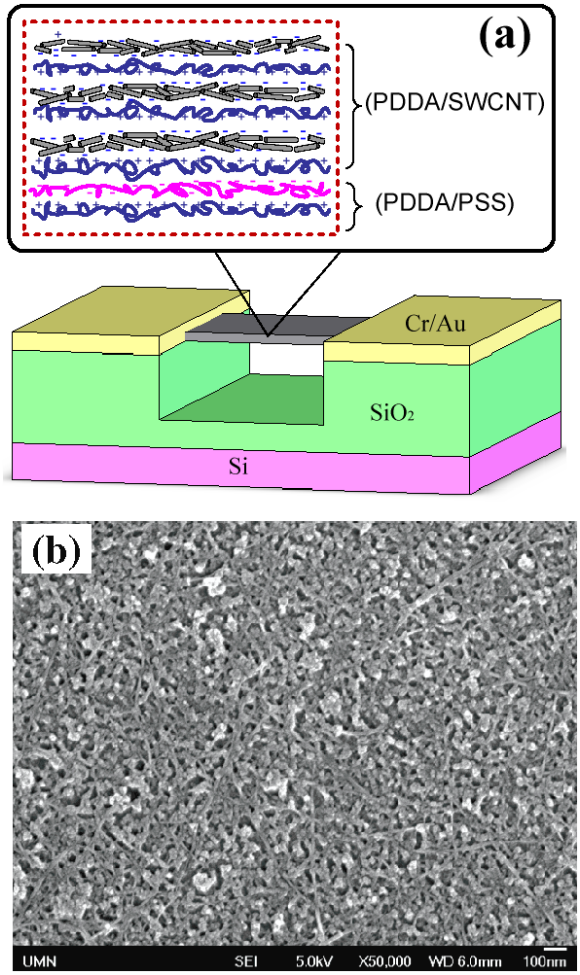

Figure 3. The release of SWCNT thin film: (a) three-dimensional schematic with a close-up thin film hierarchy and (b) top-view SEM image of the suspended SWCNT thin film fabricated by LbL self-assembly, micropatterning by lithography, and sacrificial SiO_2 layer etching.

Raman spectroscopy was performed on the SWCNT composite film and etched region as illustrated in figure 2(c). The Raman spectra on the SWCNT composite micropattern and etched region, in figure 2(d), reveal that SWCNTs have been completely removed by O_2 plasma etching. The main feature of the spectrum on the SWCNT composite pattern is the Raman shift at 164 cm^{-1}, which is in the radial breathing mode (RBM), where all atoms of the SWCNT vibrate radially in phase. It is widely known that the RBM is dependent only on the SWCNT diameter through the following equation [29]:

$$\omega_{\mathrm{RBM}} = \frac{A}{d} + B$$

where ω_{RBM} is the Raman shift at RBM, d is the diameter of the SWCNT, and A and B are constants. Based on the reported values of $A = 204$ cm^{-1} nm and $B = 27$ cm^{-1} [30], the diameter of SWCNTs used in this study has been determined as 1.5 nm, which is in good agreement with the material data. The other characteristic peaks are the most intensive energy mode at 1591 cm^{-1} (G-mode), the defect induced D-mode at 1310 cm^{-1}, and the G′-mode at 2604 cm^{-1}, which

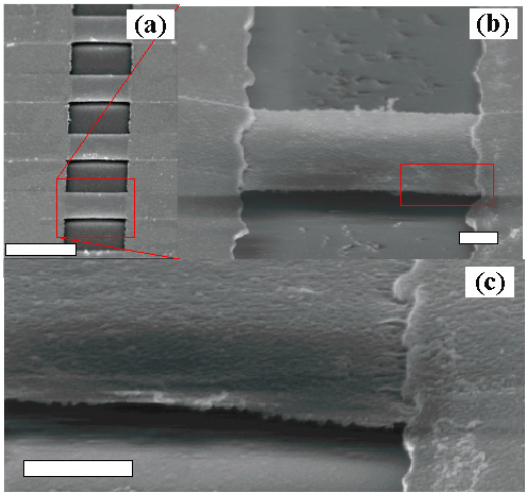

Figure 4. 60° tilted SEM images of the suspended SWCNT beam (8 μm long, 5 μm wide and 78 nm thick): (a) beam array (scale bar: 10 μm), (b) an individual beam (scale bar: 1 μm) and (c) enlarged image on anchor (scale bar: 1 μm): the gap between the suspended SWCNT multilayer and the oxide surface is clearly observable in (b).

are all evidence of the presence of SWCNTs [29]. However, none of those characteristic peaks were found on the etched region, even though the signal collection time increased to 60 s. Peaks found at 525 and 954 cm^{-1} in both spectra are caused by the Si/SiO_2 substrate, which increased with the signal collection time. Consequently, Raman spectra in figure 2(d) demonstrated that SWCNTs have been completely removed by O_2 plasma, which suggests the lithographically-compatible incorporation of CNTs.

The structure of the suspended SWCNT composite film beam is illustrated in figure 3. A three-dimensional schematic of suspended beam is shown in figure 3(a) along with a close-up of the thin film structure. The beam has a structural layer of $(PDDA/SWCNT)_{10}$ with a metal 'clamp' on both ends, which sustains the assumption of a fixed–fixed beam for the mechanical characterization later. Furthermore, a metal 'electrode' was used to measure the electrical properties and electromechanical behavior during the indentation test. The thickness of the multilayer film was 78 nm, which was measured by a surface profiler before release. A top-view SEM image of a suspended thin film is shown in figure 3(b), where the individual SWCNTs, bundles, and random network are observed.

HF vapor tends to be instilled into SWCNT composite film as well as the exposed oxide surface, which facilitates the release of the thin film. Tilted SEM images of the suspended beam array and individual beam are shown in figures 4(a) and (b), respectively, where the gap between

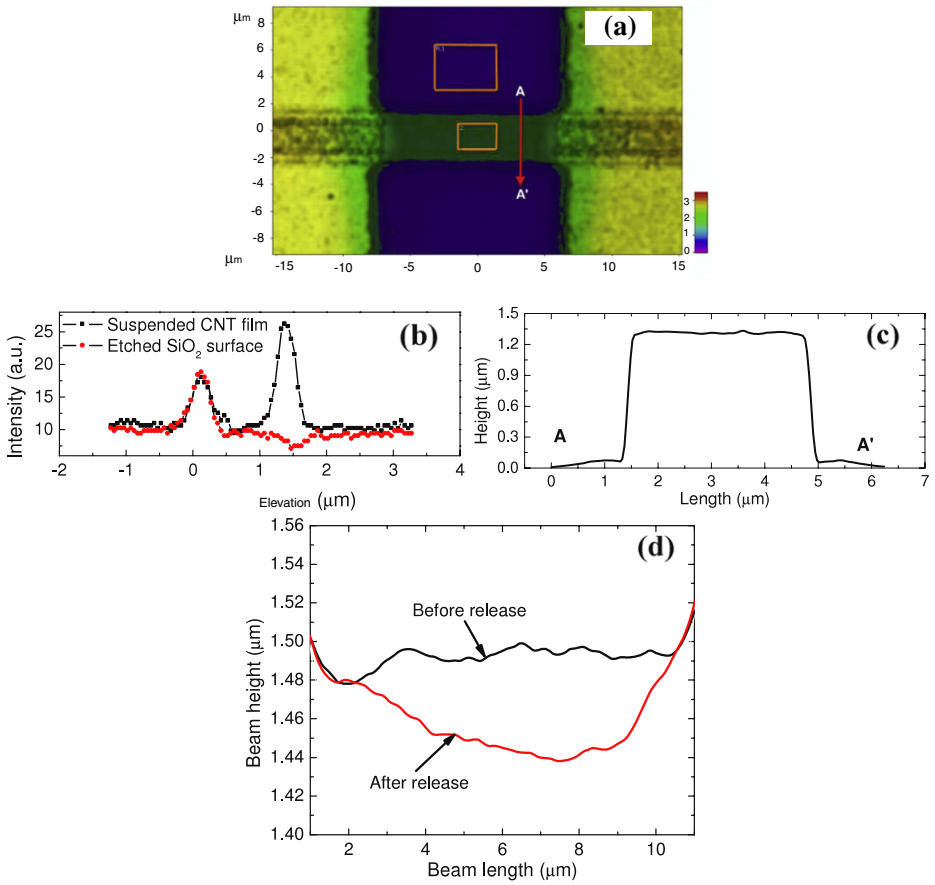

Figure 5. Characterization of a suspended SWCNT beam with confocal microscopy: (a) topographical image of the suspended SWCNT beam with 1.29 μm height difference between two rectangles; (b) reflected light intensity while the sample stage moves vertically showing two peaks on the suspended beam and one peak on the etched oxide surface; (c) surface profile along A–A′ where 1.3 μm of step height is observed; and (d) beam profile along the length before and after release.

SWCNT composite beams and the etched oxide surface is clearly observable. Furthermore, a good mechanical anchor is observed between the SWCNT composite beam and sputtered metal, as shown in figure 4(c). However, it is still doubtful if the oxide has been completely removed from underneath the beam center, which could be characterized by confocal microscopy.

Confocal microscopy was used to study the topology of the suspended beam as shown in figure 5. A reconstructed confocal micrograph of the suspended beam is shown in figure 5(a), where the averaged elevation on the suspended film and etched oxide surface represented as two rectangles showing the height difference of 1.29 μm. Also the reflection intensity was extracted inside two rectangles at different elevations and depicted in figure 5(b). On the suspended SWCNT nanocomposite beam there are two peaks observed at the elevation of 0.1 and 1.4 μm, whereas one peak is observed on the etched oxide surface at an elevation of 0.1 μm. Since the SWCNT composite film is ultra-thin, the ultra-violet (UV) light penetrates into the suspended beam, reaching the etched bottom surface. Therefore, two reflective peaks can be observed on the suspended beam at different elevations. The existence of two peaks all over the suspended beam confirms the complete release of the beam, which was doubtful in tilted SEM images. The major peak at 1.4 μm elevation is ascribed to the SWCNT film surface and the minor peak at 0.1 μm elevation is due to the etched bottom surface. Therefore, the topographical information in figure 5(a) was constructed based on major peaks. The height profile along A–A′ in figure 5(a) was extracted and is illustrated in figure 5(c). The height is referenced to the etched oxide surface and the step height was found to be 1.3 μm. In addition, height information was extracted, as shown in figure 5(d), along the beam length using the major peak before and after beam release. A beam deflection of about 50 nm was induced near the center upon release.

The suspended beams were characterized electrically using I–V measurement as shown in figure 6. The representative I–V curves for a 10 μm long, 5 μm wide, and 78 nm thick beam before and after release are shown in figure 6(a). Both curves showed Ohmic contact behavior between the metal electrodes and the SWCNT composite film. The resistance of 31.3 kΩ before release decreased to 20 kΩ after release even though there was induced deflection as shown in figure 5(d). The histogram in figure 6(b) was fitted to the normal distribution, yielding a mean value of 23%. It was reported that two kinds of mechanism of electrical conductance change played an important role in the CNT–polymer composite [31, 32]: a tunneling effect among neighboring CNTs and CNT reorientation. For a small deflection of the suspended beam upon release, SWCNTs might be preferentially oriented slightly along the length direction, which would reduce the resistance. However, at large deflection, as discussed later, the interconnection among CNTs changes, resulting in the tunneling effect among neighboring CNTs becoming dominant.

The mechanical characterization was performed by employing nanoindentation with a scanning capability, as

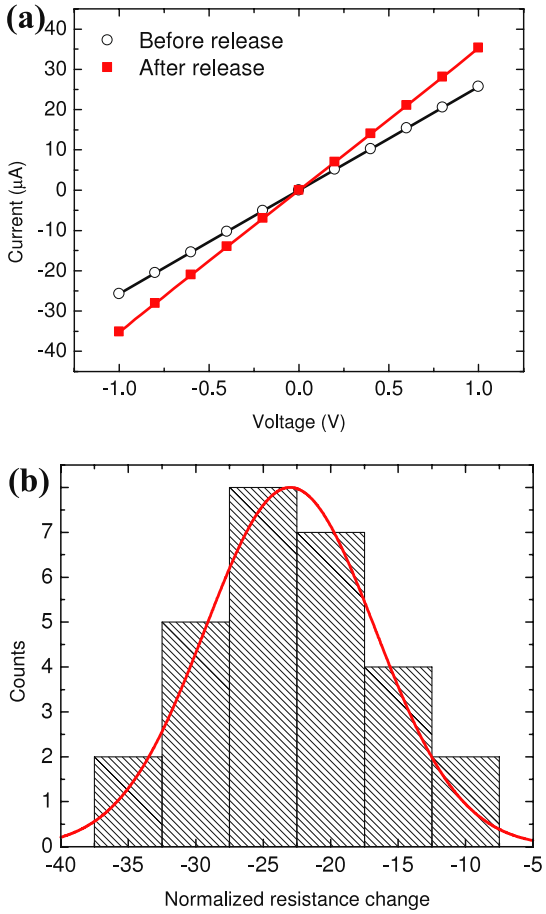

Figure 6. Electrical characterization: (a) representative I–V curves of the SWCNT micropattern (10 μm long, 5 μm wide, and 78 nm thick) before/after release and (b) statistical distribution of normalized resistance changes with the fitted normal distribution curve: the resistance of SWCNT thin film tends to decrease by an average of 23%.

shown in figure 7(a). The two-wire resistance measurement was used to monitor the beam deflection. Firstly, the suspended beams were roughly located using an optical microscope as shown in figure 7(b), where the crossover indicates the location of the indenter tip by optic-to-tip calibration. The sample surface was scanned to find the center of the suspended beam with a force of 2 μN. Firstly, the control samples of an etched oxide surface and collapsed SWCNT composite film beam made using buffered oxide etching (BOE) for the sacrificial layer etching were tested. The collapsed composite beam is the beam that had been stuck down onto the etched oxide surface. The spring constants of the collapsed composite beam and SiO_2 surface were extracted in the same way as done for suspended composite beams and used as reference values to compare with those of a suspended composite beam. The load function used was a linear increase to maximum load for 10 s and a linear decrease to zero for 10 s. The spring constant was extracted from 30–95% of maximum load while unloading in the force–deflection (F–δ) curve. The result of mechanical testing of the control samples shows the spring constants are in the range of tens of μN nm^{-1} as shown in figure 7(c). The example of a scanned image of a beam

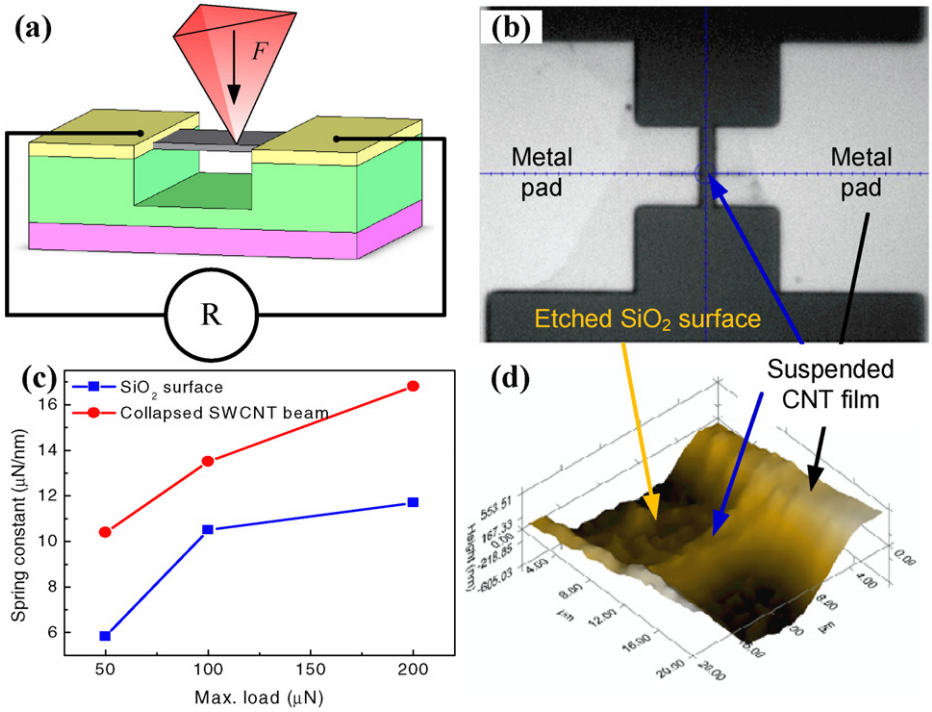

Figure 7. Mechanical characterization of a suspended beam by nanoindentation: (a) nanoindentation testing setup with two-wire resistance measurement; (b) optical image of the testing platform; (c) spring constants of control samples extracted from force–deflection curves while unloading; and (d) scanned image of the suspended SWCNT beam: scanning of the sample surface starts from the center of the image in (b). The location of the tip can be narrowed down by scanning the surface as in (d). Once the center of beam is placed at the image center in (d), the load function is applied to get force–deflection curves.

suspended from nanoindenter is shown in figure 7(d). The indenter used here was a Berkovich tip with a tip radius of about 1 μm to ensure that the indenter does not penetrate the SWCNT composite film so that the deflection measured in the indentation test can be considered as the total beam deflection. We assumed the range of the elastic deformation in the SWCNT composite film is much smaller than that of composite beam deflection. The elastic deformation and composite beam deflection are modeled as two springs in series, where the spring corresponding to elastic deformation is much stiffer than the one corresponding to beam deflection, considering the four orders higher spring constant of collapsed composite beams.

A typical force–deflection (F–δ) curve for the suspended beam with dimensions of 15 μm length, 5 μm width and 78 nm thickness is shown in figure 8(a). It is noted that the LbL assembled CNT composite beam exhibited a large deflection, about three times the beam thickness, while maintaining a linear response. Most F–δ curves demonstrated the linear region from which the spring constant (k) of the suspended beam was extracted. Specifically, the spring constants for one sample were found while unloading and averaged from multiple loading/unloading cycles as shown in figure 8(b). Ultimately, the averaged spring constant (k) of 7.32 ± 1.67 N m^{-1} was found from multiple samples. This is almost four orders smaller than that found in control samples, as shown in figure 7(c). Using an Euler beam model with fixed ends enduring a point load at the center, the Young's modulus (E) of the SWCNT–polymer composite can be extracted as follows based on the rectangular beam cross section:

$$E = \frac{L^3 k}{16 w t^3}$$

where, L, w, and t represent the length, width, and thickness of beam, respectively. E was calculated to have the nominal value of 650 GPa. Considering that the maximum thickness variation was 2.0 nm along with the standard deviation of the spring constants extracted, a range of 500–800 GPa is expected. Moreover, in response to the force curve in figure 8(b), temporal changes in beam deflection and resistance are depicted in figure 8(c). The resistance of a suspended beam follows the trend of beam deflection, demonstrating piezoresistive behavior. The resistance decreases by 60 Ω when the beam is deflected by 110 nm by the application of a 0.7 μN force. The deflection–responsive resistance change can be explained by the reduced tunneling effect due to decreased interconnections among SWCNTs or by the mechanical deflection of individual SWCNTs [33, 34]. One of possible reasons for a high Young's modulus is that LbL assembly can attain a high loading of CNTs compared to the other methods mentioned for fabricating CNT–polymer composites. For instance, it is estimated that 63% of the volume and 74% of the mass of CNTs are contained in the LbL film based on the quartz crystal microbalance monitoring of LbL growth [25]. Furthermore, during LbL assembly, nonspecifically and weakly bound CNTs are removed by thorough immediate washing, followed by the deposition of a polymer as an adhesive to increase surface charge. In this way,

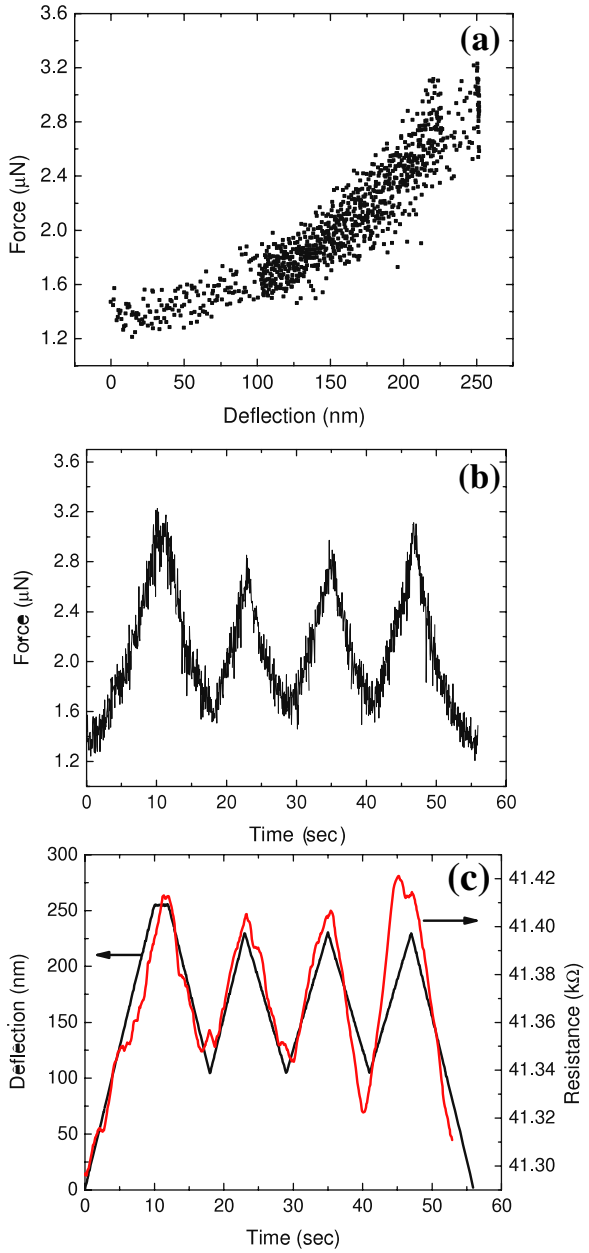

Figure 8. The result of mechanical testing of a suspended SWCNT beam (15 μm long, 5 μm wide and 78 nm thick): (a) a typical force (f) versus deflection curve (δ), (b) load function that contains multiple load/unload cycles, and (c) temporal changes of deflection of the beam and the resistance of suspended beam.

molecular LbL assembly can make a stiff material without any segregation.

4. Conclusion

The fabrication and characterization of SWCNT composite film micropatterns and suspended beams have been presented. The micropattern was fabricated using oxygen plasma etching with a photoresist mask and a feature size of 2 μm was identified with optical microscopy and SEM. Raman spectroscopy showed that SWCNT composite were completely removed in the etched region. The release of SWCNT composite film was realized by HF vapor etching to avoid stiction and evidenced by SEM and confocal microscopy. For electrical characterization, I–V measurement indicated that the resistance of the SWCNT composite film decreased upon release. The suspended beam showed a Young's modulus of 650 GPa following indentation testing based on a fixed–fixed beam. This is higher than the values reported for CNT–polymer composites, presumably due to the high loading of CNTs and organized structure via the molecular level LbL assembly. The stiff CNT composite micropattern and suspended CNT composite beam may have potential applications in novel physical sensors, nanoelectronics, nanoelectromechanical switches, other M/NEMS devices, etc.

Acknowledgments

This work was partially supported by the DARPA M/NEMS Science and Technology Fundamentals Program through the Micro/nano Fluidics Fundamentals Focus (MF3) Center. The authors would like to acknowledge the Nanofabrication Center, University of Minnesota, which is supported by NSF through NNIN. Parts of this work were carried out in the Institution of Technology Characterization Facility, University of Minnesota.

References

[1] Han J 2004 *Carbon Nanotubes: Science and Application* ed M Meyyappan (New York: CRC Press) pp 8–24
[2] Rueckes T, Kim K, Joselevich E, Tseng G Y, Cheung C-L and Lieber C M 2000 *Science* **289** 94–7
[3] Wind S J, Appenzeller J, Martel R, Derycke V and Avouris P 2002 *Appl. Phys. Lett.* **80** 3817–9
[4] Tans S J, Verschueren A R M and Dekker C 1998 *Nature* **393** 49–52
[5] Kong J, Franklin N R, Zhou C, Chapline M G, Peng S, Cho K and Dai H 2000 *Science* **287** 622–5
[6] Lee D and Cui T 2010 *Biosens. Bioelectron.* **25** 2259–64
[7] Yan Y, Chan-Park M B and Zhang Q 2007 *Small* **3** 24–42
[8] Cao J, Wang Q, Wang D and Dai H 2005 *Small* **1** 138–41
[9] Ren Z F, Huang Z P, Xu J W, Wang J H, Bush P, Siegal M P and Provencio P N 1998 *Science* **282** 1105–7
[10] Hua F, Cui T and Lvov Y M 2004 *Nano Lett.* **4** 823–5
[11] Xue W and Cui T 2007 *Sensors Actuators* A **136** 510–7
[12] Sandler J, Shaffer M S P, Prasse T, Bauhofer W, Schulte K and Windle A H 1999 *Polymer* **40** 5967–71
[13] Biercuk M J, Llaguno M C, Radosavljevic M, Hyun J K, Johnson A T and Fischer J E 2002 *Appl. Phys. Lett.* **80** 2767–9
[14] Liu C H, Huang H, Wu Y and Fan S S 2004 *Appl. Phys. Lett.* **84** 4248–50
[15] Scardaci V, Rozhin A G, Hennrich F, Milne W I and Ferrari A C 2007 *Physica* E **37** 115–8
[16] Lu J P 1997 *Phys. Rev. Lett.* **79** 1297–300
[17] Yao N and Lordi V 1998 *J. Appl. Phys.* **84** 1939–43
[18] Qian D, Dickey E C, Andrews R and Rantell T 2000 *Appl. Phys. Lett.* **76** 2868–70
[19] Ajayan P M, Schadler L S, Giannaris C and Rubio A 2000 *Adv. Mater.* **12** 750–3
[20] Tang W, Santare M H and Advani S G 2003 *Carbon* **41** 2779–85
[21] Barraza H J, Pompeo F, O'Rea E A and Resasco D E 2002 *Nano Lett.* **2** 797–802
[22] Kim Y, Minami N, Zhu W, Kazaoui S, Azumi R and Matsumoto M 2003 *Japan. J. Appl. Phys.* **42** 7629–34

[23] Mamedov A A, Kotov N A, Prato M, Guldi D M, Wicksted J P and Hirsch A 2002 *Nat. Mater.* **1** 190–4
[24] Xue W, Liu Y and Cui T 2006 *Appl. Phys. Lett.* **89** 163512
[25] Xue W and Cui T 2007 *Nanotechnology* **18** 145709
[26] Chae J, Ho X, Rogers J A and Jain K 2008 *Appl. Phys. Lett.* **92** 173115
[27] Lee D and Cui T 2009 *IEEE Sensors J.* **9** 449–56
[28] Lee D and Cui T 2009 *J. Vac. Sci. Technol.* B **27** 842–8
[29] Graupner R 2007 *J. Raman Spectrosc.* **38** 673–83
[30] Meyer J C, Paillet M, Michel T, Moreac A, Neumann A, Duesberg G S, Roth S and Sauvajol J-L 2005 *Phys. Rev. Lett.* **95** 217401
[31] Hu N, Karube Y, Yan C, Masuda Z and Fukunaga H 2008 *Acta Mater.* **56** 2929–36
[32] Hu N, Karube Y, Arai M, Watanabe T, Yan C, Li Y, Liu Y and Fukunaga H 2010 *Carbon* **48** 680–7
[33] Tombler T W, Zhou C, Alexseyev L, Kong J, Dai H, Liu L, Jayanthi C S, Tang M and Wu S-Y 2000 *Nature* **405** 769–72
[34] Xue W and Cui T 2008 *Sensors Actuators* A **145/146** 330–5